

AEGIS: NEW EVIDENCE LINKING ACTIVE GALACTIC NUCLEI TO THE QUENCHING OF STAR FORMATION

KEVIN BUNDY¹, ANTONIS GEORGAKAKIS^{2,3}, KIRPAL NANDRA², RICHARD S. ELLIS⁴, CHRISTOPHER J. CONSELICE^{4,5}, ELISE LAIRD², ALISON COIL^{6,7}, MICHAEL C. COOPER^{6,8}, SANDRA M. FABER⁹, JEFF A. NEWMAN¹⁰, CHRISTY M. PIERCE¹¹, JOEL R. PRIMACK¹¹, RENBIN YAN¹⁰

submitted to ApJ

ABSTRACT

Utilizing *Chandra* X-ray observations in the All-wavelength Extended Groth Strip International Survey (AEGIS) we identify 241 X-ray selected Active Galactic Nuclei (AGNs, $L_{2-10\text{keV}} > 10^{42}$ ergs s^{-1}) and study the properties of their host galaxies in the range $0.4 < z < 1.4$. By making use of infrared photometry from Palomar Observatory and *BRI* imaging from the Canada–France–Hawaii Telescope, we estimate AGN host galaxy stellar masses and show that both stellar mass and photometric redshift estimates (where necessary) are robust to the possible contamination from AGNs in our X-ray selected sample. Accounting for the photometric and X-ray sensitivity limits of the survey, we construct the stellar mass function of X-ray selected AGN host galaxies and find that their abundance decreases by a factor of ~ 2 since $z \sim 1$, but remains roughly flat as a function of stellar mass. We compare the abundance of AGN hosts to the rate of star formation quenching observed in the total galaxy population. If the timescale for X-ray detectable AGN activity is roughly 0.5–1 Gyr—as suggested by black hole demographics and recent simulations—then we deduce that the inferred AGN “trigger” rate matches the star formation quenching rate, suggesting a link between these phenomena. However, given the large range of nuclear accretion rates we infer for the most massive and red hosts, X-ray selected AGNs may not be *directly* responsible for quenching star formation.

Subject headings: cosmology: observations, galaxies: formation, galaxies: evolution

1. INTRODUCTION

Recent observations of the galaxy population and its evolution since $z \approx 2$ reveal a pattern in which the most massive galaxies appear to shut down star formation activity at early times with increasingly less massive galaxies following later (e.g., Juneau et al. 2005; Treu et al. 2005; Bundy et al. 2006; Borch et al. 2006; Cimatti et al. 2006). This pattern of “quenching” in the star formation history of galaxies—thought to be largely responsible for the growing abundance of galaxies on the red sequence (e.g., Faber et al. 2007)—is commonly referred to as “downsizing” (Cowie et al. 1996).

Given that the dark matter halos of galaxies are expected to assemble hierarchically in the Λ CDM paradigm, understanding the physical mechanisms responsible for downsizing remains an important challenge.

We seek a process capable of quenching star formation, driving galaxies onto the red sequence, and preventing further star formation. Work with the DEEP2 Galaxy Redshift Survey (Davis et al. 2003) has shown that such a process must operate over a range of environmental densities (Bundy et al. 2006; Cooper et al. 2007; Gerke et al. 2007), suggesting an internal component to quenching that acts in addition to the suppression of star formation expected in high-density environments. Meanwhile, theoretical work has focused on one such internal process, namely the potential role played by AGN feedback (Silk & Rees 1998), both as a way of explosively initiating the quenching event (Granato et al. 2004; Scannapieco et al. 2005; Hopkins et al. 2005a) and preventing hot gas in already passive galaxies from cooling to form stars (Croton et al. 2006; Bower et al. 2006; Cattaneo et al. 2006; de Lucia & Blaizot 2007).

These scenarios remain largely untested because observational evidence has been difficult to obtain. One of the most promising ways forward is to examine the properties of AGN host galaxies and search for signatures of this feedback. Such observations are challenging however because no selection method finds all galaxies that host active nuclei (Mushotzky 2004) and brighter AGNs (quasars) can easily outshine their hosts. With such difficulties in mind, previous studies suggest that most lower luminosity AGNs tend to be found in massive, mostly spheroidal galaxies (Dunlop et al. 2003; Kauffmann et al. 2003; Grogin et al. 2005; Pierce et al. 2007) although some “transition” sources exhibit disturbed morphologies (e.g., Canalizo & Stockton 2001; Hutchings et al. 2006; Conselice et al. 2007). AGNs detected through emission line diagnostics and X-rays ap-

¹ Reinhardt Fellow, Dept. of Astronomy and Astrophysics, University of Toronto, 50 St. George Street, Rm 101, Toronto, ON M5S 3H4, Canada

² Astrophysics Group, Blackett Laboratory, Imperial College, London SW7 2AZ, UK

³ Marie Curie Fellow

⁴ 105–24 Caltech, 1201 E. California Blvd., Pasadena, CA 91125

⁵ University of Nottingham, School of Physics & Astronomy, Nottingham, NG72RD UK

⁶ Steward Observatory, University of Arizona, 933 N. Cherry Avenue, Tucson, AZ 85721 USA

⁷ Hubble Fellow

⁸ Spitzer Fellow

⁹ University of California Observatories/Lick Observatory, Board of Studies in Astronomy and Astrophysics, University of California, Santa Cruz, CA 95064

¹⁰ Department of Astronomy, University of California at Berkeley, MC 3411, Berkeley, CA 94720

¹¹ Department of Physics, University of California, Santa Cruz, 1156 High Street, Santa Cruz, CA 95064, USA

pear to prefer host galaxies on the red sequence and “green valley” (Nandra et al. 2007; Martin et al. 2007; Salim et al. 2007).

Further progress on testing the link between AGN activity and the downsizing of star formation requires that we understand the stellar mass distribution and redshift evolution of AGN hosts as compared to evolutionary patterns in the general galaxy population. In this paper we use deep *Chandra* observations to identify AGN hosts in the AEGIS field (Davis et al. 2007) where spectroscopic and photometric redshifts (photo- z ’s) as well as infrared photometry provide reliable stellar mass estimates out to $z = 1.4$. We then compute the AGN host stellar mass function and use it to estimate the rate at which AGN activity is triggered in the galaxy population. We will show that this mass-dependent rate is consistent with the rate of star formation quenching of all galaxies at the same epochs at which the AGN activity is observed.

The structure of the paper is as follows. We describe the multi-wavelength observations and properties of the sample in §2 and §3. The way in which stellar masses and restframe colors are determined is given in §4 while our methods for constructing mass functions and the resulting AGN host mass function are presented in §5. In §6 we present evidence for a link between AGN activity and quenching in the context of estimates of the X-ray AGN timescale and explore whether feedback from X-ray selected AGNs causes quenching. We summarize in §7. Where necessary, we assume a standard cosmological model with $\Omega_M = 0.3$, $\Omega_\Lambda = 0.7$, $H_0 = 70h_{70}$ km s $^{-1}$ Mpc $^{-1}$.

2. OBSERVATIONS

In this section, we discuss the various observations we use to investigate the link between AGNs and galaxy evolution. We begin by summarizing the DEEP2 Galaxy Redshift Survey (Davis et al. 2003) and a followup infrared imaging campaign conducted at Palomar Observatory. One of the four fields in this survey, the Extended Groth Strip (EGS), was imaged with *Chandra* as part of the AEGIS program, providing a sample of AGN host galaxies that we utilize here. We will compare the evolution of this AGN host sample to trends observed in galaxies drawn from the full DEEP2/Palomar survey. As discussed in Bundy et al. (2006), this sample provides robust stellar mass estimates that can be used to investigate mass-dependent evolution out to $z = 1.4$.

2.1. The DEEP2/Palomar Survey

We provide a brief summary of the DEEP2 Galaxy Redshift survey and the near-infrared (IR) followup imaging conducted at Palomar Observatory. The data sets involved were utilized by Bundy et al. (2006) to explore the nature of star formation downsizing since $z \approx 1.2$, and further details are provided there. Now complete, the DEEP2 Galaxy Redshift survey (Davis et al. 2003) utilized DEIMOS on the Keck-II telescope to obtain spectroscopic redshifts for $\sim 40,000$ galaxies with $z \lesssim 1.5$. The survey is magnitude limited at $R_{AB} \leq 24.1$ and covers more than 3 square degrees over four fields, one of which is the AEGIS field and is described further below.

Redshift targets were selected using *BRI* photometry from the Canada–France–Hawaii Telescope (CFHT) with

the 12K \times 8K mosaic camera (Cuillandre et al. 2001). As described in Coil et al. (2004), the photometry reaches $R_{AB} \sim 25.5$ and was also used for estimating photo- z ’s and restframe ($U - B$) colors, as discussed below. In the three non-AEGIS fields, target selection in DEEP2 was carried out using observed colors to exclude sources with $z < 0.7$. These selection criteria successfully recover 97% of the $R_{AB} \leq 24.1$ population at $z > 0.75$ with only $\sim 10\%$ contamination from lower redshift galaxies (Davis et al. 2005). More details on the observing strategy and characteristics of the DEEP2 sample are provided in Coil et al. (2004), Willmer et al. (2006), Davis et al. (2005), Faber et al. (2007), Davis et al. (2007), and Newman et al. (in preparation).

Followup imaging of the DEEP2 survey in the J and K_s -band were carried out using Wide Field Infrared Camera (WIRC, Wilson et al. 2003) on the 5m Hale Telescope at Palomar Observatory. These observations are discussed in detail in Bundy et al. (2006). Excluding the AEGIS field, which was the highest priority, 0.9 square degrees of DEEP2 were imaged primarily in the K_s -band with exposure times varying from 2 to 8 hours, depending on the conditions, and the final typical 80% completeness depth of $K_{AB} = 21.5$.

We used SExtractor (Bertin & Arnouts 1996) to detect and measure K_s -band sources and cross-referenced them with the CFHT optical and DEEP2 redshift catalogs to construct a K-selected sample that forms the basis of our analysis. For total magnitudes used to estimate stellar masses, we took the MAG_AUTO output from SExtractor and did not correct this Kron-like magnitude for missing light. We estimated the uncertainty on these magnitudes by inserting fake sources at various magnitudes and using SExtractor to recover them. Based on the locations of K-selected sources, we measured aperture photometry in the *BRI* data using 2” diameter apertures which we found exhibited the least scatter. These colors are used in fitting galaxy spectral energy distributions (SEDs) needed for both photo- z ’s and stellar mass estimates.

2.2. The AEGIS Field

Covering the 0.5 deg 2 Extended Groth Strip ($\alpha = 14^{\text{h}}17^{\text{m}}, \delta = +52^{\circ}30'$), the All-Wavelength Extended Groth Strip International Survey (AEGIS, Davis et al. 2007) accounts for one of the four fields where DEEP2 redshifts and Palomar near-IR imaging were obtained, although there are slight differences with respect to the other DEEP2 fields (above) that we describe here. This field is also special because many other observatories, including the *Hubble* and *Spitzer Space Telescopes*, have conducted observations there. Of key importance for this work are the deep X-ray data from the Advanced CCD Imaging Spectrometer (ACIS) on *Chandra*.

The *Chandra* data are described in Georgakakis et al. (2006) and Georgakakis et al. (2007b), and the X-ray data analysis is presented in Nandra et al. (2005). Briefly, the AEGIS region was targeted over several epochs for a total integration time of 190 ks. Standard reduction methods using the CIAO software were employed to derive fluxes in four energy bands—0.5–7.0 keV (full), 0.5–2.0 keV (soft), 2.0–7.0 keV (hard), and 4.0–7.0 (ultrahard)—by integrating the counts detected

within the 70% encircled energy radius at each source position. The counts in each observed band were converted to the standard bands of 0.5–10, 0.5–2, 2–10, and 5–10 keV by assuming an intrinsic power-law with $\Gamma = 1.4$ and Galactic absorption. The typical detection limits in each band are 35, 1.1, 8.2, and 14 in units of 10^{-16} ergs $s^{-1} cm^{-2}$, although these depend on position because the *Chandra* sensitivity declines away from the center of each pointing. X-ray detections were referenced to the optical/IR photometric catalogs using the method described in Georgakakis et al. (2006).

In terms of the DEEP2 spectroscopic redshifts, target selection was carried out differently in AEGIS than it was in the other DEEP2 fields. Here, a straight magnitude limit of $R_{AB} \leq 24.1$ was employed with galaxies having $z \lesssim 0.7$ down-weighted but not excluded from the target sample. The near-IR Palomar imaging is deepest in EGS, especially along the center of the strip where *J*-band imaging was also obtained, and the typical 80% completeness depth is $K_{AB} = 22.5$. Overall, the typical AEGIS depth reaches $K_{AB} \approx 22$. The properties of the CFHT *BRI* data are identical to those described above.

3. THE GALAXY AND AGN HOST SAMPLES

To begin our analysis of AGN hosts and their relationship to evolution in the galaxy population we distinguish between the *galaxy sample* and the *AGN host sample*. The galaxy sample is comprised of the full DEEP2/Palomar survey, including the AEGIS. With the goal of providing a self-consistent benchmark for AGN host comparisons, we note that this sample is slightly larger than the one presented in Bundy et al. (2006) because unlike that paper, our analysis does not require that we restrict the perimeter of the survey on account of accurate environmental density measurements. While X-ray observations are not required for the galaxy sample, we do select sources in the K_s -band with good quality (“zquality” ≥ 3 , see Davis et al. 2007) spectroscopic redshifts in the redshift range $0.4 < z < 1.4$, reaching K_s -band limits that depend on redshift. As in Bundy et al. (2006), we use $K_{AB} \leq 21.8, 22.0, 22.2$ for $z \leq 0.7, 1.0, 1.4$.

We apply the same limits to the AGN host galaxies which are identified in the *Chandra* full band and have a Poisson false detection probability that is less than 4×10^{-6} . We then use the redshift of the matched host and assume $\Gamma = 1.9$ to infer L_{2-10} , the X-ray luminosity in the 2–10 keV energy band. This effectively corrects for absorption for column densities of $N_H \lesssim 10^{23} cm^{-2}$ at $z \approx 1$ (Nandra & Pounds 1994), and we apply this procedure even if the source is not detected in the hard band.

AGNs are identified as those sources with $L_{2-10} > 10^{42}$ ergs s^{-1} ; we note that AGNs are certainly present in sources below this threshold, although they are more difficult to distinguish with the present data. Because normal galaxies without AGNs have not been observed with $L_{2-10} > 10^{42}$ ergs s^{-1} (see Bauer et al. 2004), we adopt this limit to ensure that there is little to no contamination from sources without AGNs. Indeed, even without an X-ray luminosity threshold, the flux limit of the *Chandra* data (8.2×10^{-16} ergs $s^{-1} cm^{-2}$ in the hard band) suggests a very low non-AGN contamination rate of only a few percent in the observed source densities (Bauer et al. 2004).

While hard X-ray selection provides one of the cleanest ways to select AGNs at high redshift (e.g., Mushotzky 2004; Barger et al. 2005), it will still miss Compton-thick sources ($N_H \gtrsim 10^{24} cm^{-2}$), which, while not expected to outnumber hard X-ray detected AGNs, are thought to contribute at least half as many (e.g., Treister & Urry 2006; Guainazzi et al. 2005; Gilli et al. 2007). We will account for missed Compton-thick AGNs by incorporating the detection efficiency of our sample in the analysis in §6.

In what follows, we will consider the AGN host sample with spectroscopic redshifts and $R_{AB} \leq 24.1$ (the spec- z sample, 84 sources) as well as a deeper sample ($R_{AB} \leq 25.1$) of AGN hosts supplemented with photometric redshifts (the photo- z sample, 241 sources). As in Bundy et al. (2006), photometric redshifts in AEGIS were estimated using two methods. For galaxies with $R_{AB} \leq 24.1$ we use ANN z (Collister & Lahav 2004), a neural network redshift estimator, which benefits from a large training set provided by the magnitude-limited nature of the DEIMOS target selection in the EGS. We also include host galaxies with $24.1 < R_{AB} \leq 25.1$ and 3σ detections in the *BIK* bands, but use the BPZ SED-based estimator (Benítez 2000) for these sources. By comparing these photo- z ’s to the DEEP2 spectroscopic redshifts we find $\delta z/(1+z) = 0.11$. Further details on these two methods as applied to galaxies in the DEEP2/Palomar sample can be found in Bundy et al. (2006). Photometric redshifts in the EGS based on the CFHT Legacy Survey are also available from Ilbert et al. (2006). Comparing these estimates to the DEEP2 spectroscopic redshifts we find $\delta z/(1+z) = 0.17$ and therefore use the slightly better ANN z +BPZ estimates described above. Note that Ilbert et al. (2006) redefine $\delta z/(1+z)$ as $1.48 \times \text{median}|z_{\text{spec}} - z_{\text{phot}}|/(1+z_{\text{spec}})$ and that with this definition the comparison to DEEP2 yields $dz_{\text{Ilbert}} = 0.03$, similar to the accuracy reported in Ilbert et al. (2006).

An obvious concern with photometric redshift estimates for AGN hosts is that non-thermal contamination could lead to large redshift errors. By comparing photometric and spectroscopic redshift estimates in the AGN spec- z host sample in Figure 1 we show that in general this is not the case. Since the global sample of galaxies ($0.4 < z_{\text{phot}} < 1.4$) is characterized by the same $\delta z/(1+z) = 0.11$, this comparison demonstrates that photometric redshifts of X-ray selected AGN hosts can be believed at the same level as those of non-AGN galaxies. This implies that AGN contamination in the optical/IR is not significant, as expected (e.g., Barger et al. 2005). Figure 1 does show, however, that the photo- z outliers are dominated by the more X-ray luminous systems, suggesting more contamination in these cases. Caution must be used in interpreting the properties of these sources.

4. PHYSICAL PROPERTIES

4.1. Restframe $U - B$ Color

Following Bundy et al. (2006) and Nandra et al. (2007), we use the methods described in Willmer et al. (2006) to estimate the restframe ($U - B$) colors in both our galaxy and AGN host samples. This measurement is frequently used as a diagnostic of star formation activity in galaxies and exhibits a bimodal distribution to at least

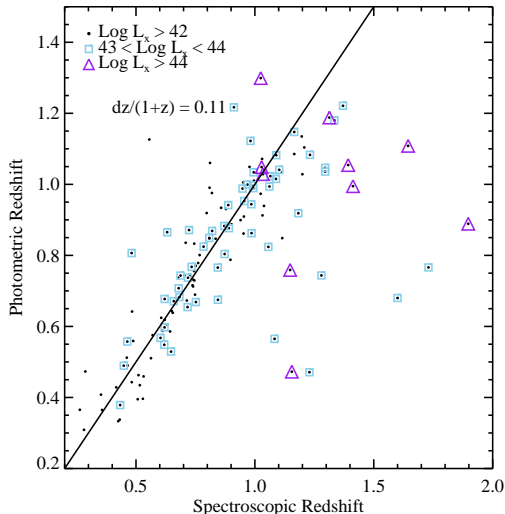


FIG. 1.— Comparison of photo- z quality for the AGN spec- z host sample. Four additional outliers with $z_{\text{spec}} > 2.0$ are not shown, and all have $L_{2-10} > 10^{43}$ ergs s^{-1} , with three having $L_{2-10} > 10^{44}$. As indicated, for $0.4 < z_{\text{phot}} < 1.4$, $\delta z/(1+z) = 0.11$, the same as the full galaxy population. We note, however, that photo- z outliers tend to be the most X-ray luminous.

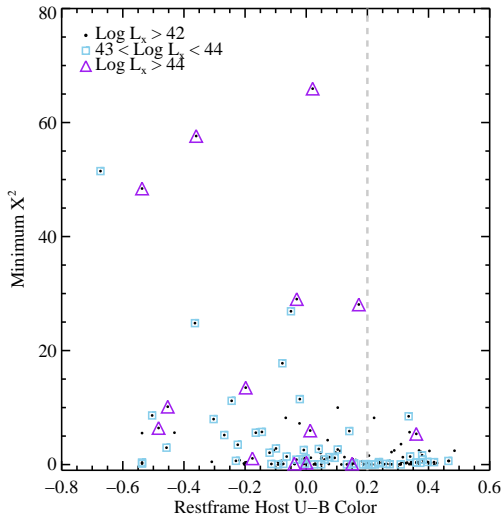


FIG. 2.— Reduced χ^2 of the best fitting SED determined by the M_* estimator as a function of restframe ($U-B$) color. More X-ray luminous AGNs tend to exhibit poorer fits, indicating the presence of AGN contamination. The blue colors of the AGN hosts of X-ray luminous sources may be caused in part by this contamination. The grey dashed line is typical of the division used to divide red and blue galaxies.

$z \sim 1$ (Bell et al. 2004), separating star-forming “blue cloud” galaxies from the mostly passive “red sequence.” We used the cut employed by van Dokkum et al. (2000) which can be expressed in Vega magnitudes as,

$$U - B = -0.032(M_B + 21.52) + 0.454 - 0.25 \quad (1)$$

The ($U - B$) color distribution for the AGN spec- z host sample is illustrated in Figure 2 and was originally discussed for a subset of the data utilized here in Nandra et al. (2007). The properties of the current and

somewhat larger sample here show agreement with those presented in Nandra et al. (2007).

4.2. Stellar Mass Estimates

To estimate stellar masses (M_*), we use the methods described in Bundy et al. (2006). Based on the observed *BRICK* colors (measured using 2"0 diameter apertures) and the redshift information for each galaxy, we fit the observed SED to a grid of 13440 models constructed using the Bruzual & Charlot (2003) population synthesis code. The grid spans a range of metallicities, star formation histories (parametrized as exponential), ages, and dust content. The grid is restricted such that only models with ages (roughly) less than the cosmic age at a galaxy’s redshift are considered. Systematic uncertainties are introduced by our choice of a Chabrier IMF (Chabrier 2003) and the use of the Bruzual & Charlot (2003) code. While some studies support M_* estimates based on the Bruzual & Charlot (2003) software (see Kannappan & Gawiser 2007), others have pointed out potential problems (Maraston et al. 2006). In Conselice et al. (2007), we show that a preliminary analysis with the latest Bruzual and Charlot models (2007, in prep.) yield mass estimates that are ~ 0.07 dex smaller on average. This issue will be discussed further in future work.

With the grid defined in this way, the SED of a given galaxy is then compared to the model at each grid point, where the specific K_s -band M_*/L_K ratios and M_* values for each model are also stored. The probability that each model fits the data is then summed or marginalized over the grid to yield the stellar mass probability distribution. The median of this distribution is taken as the estimate of M_* , and the width provides an estimate of the uncertainty, typically 0.1–0.2 dex. This is added in quadrature to the K_s -band magnitude uncertainty to determine the final error on M_* . Stellar mass estimates for galaxies with only photometric redshifts suffer from the uncertainty in luminosity distance introduced by the photo- z uncertainties and the possibility of catastrophically wrong redshift information. A study of the effect of photometric redshifts on stellar mass was performed in Bundy et al. (2005).

For the case of the AGN host samples, it is important to consider the effects of non-thermal contamination which may affect the inferred stellar masses. Including an AGN component in the model SEDs used to estimate the stellar mass is not practical. Instead we investigate the potential error by plotting the reduced χ^2 values of the best fitting SED from the stellar mass grid for each member of the AGN spec- z host sample in Figure 2. Even under the best conditions, we do not require a perfect fit to the observed SED because our Bayesian mass estimator considers a range of models when assigning the final mass estimate. Still, mass estimates with $\chi^2 > 30$ should be considered with caution. Fortunately, while the average χ^2 value of AGN hosts is higher than for galaxies without AGNs (e.g., the fraction of AGN hosts with $\chi^2 > 10$ is 10%, while this number for all galaxies is 1%) and seems to correlate with L_{2-10} , only 4 hosts have $\chi^2 > 30$, indicating that the mass estimates for the AGN host sample are robust.

5. STELLAR MASS FUNCTIONS

5.1. Methods

With the M_* estimates described above, we are now in a position to construct stellar mass functions (MFs) from our sample. We will describe our formalism in this section and present the AGN host mass function in §5.2. The same methods are also applied to construct MFs for the full galaxy sample. These allow us to study the growing fraction of red galaxies which we will use to infer the star formation quenching rate in §6.1.

Constructing galaxy stellar MFs requires understanding and correcting for the limitations and completeness of the survey data. We adopt the V_{max} formalism (Schmidt 1968) to this end, following Bundy et al. (2006). In the case of the galaxy sample, the maximum volume can be limited by either the K_s -band depth or the $R_{AB} \leq 24.1$ limit used to define the DEEP2 spectroscopic sample. In this case, for each galaxy i in the redshift interval j , the value of V_{max}^i is given by the minimum redshift at which the galaxy would leave the sample,

$$V_{max}^i = \int_{z_{low}}^{z_{high}} d\Omega_j \frac{dV}{dz} dz \quad (2)$$

where $d\Omega_j$ is the solid angle subtended by the sample defined by the limiting K_s -band magnitude, K_{lim}^j (which changes depending on the redshift interval j), and dV/dz is the comoving volume element. The redshift limits are given as,

$$z_{high} = \min(z_{max}^j, z_{K_{lim}}^j, z_{R_{lim}}^j) \quad (3)$$

$$z_{low} = z_{min}^j \quad (4)$$

where the redshift interval, j , is defined by $[z_{min}^j, z_{max}^j]$, $z_{K_{lim}}^j$ refers to the redshift at which the galaxy would still be detected below the K_s -band limit for that particular redshift interval, and $z_{R_{lim}}^j$ is the redshift at which the galaxy would no longer satisfy the R -band limit of $R_{AB} \leq 24.1$. We use the best-fit SED template as determined by the stellar mass estimator to calculate $z_{K_{lim}}^j$ and $z_{R_{lim}}^j$, thereby accounting for the k -corrections necessary to compute accurate V_{max} values (no evolutionary correction is applied).

In the case of the AGN host samples, the procedure must be modified to account for the limiting X-ray depth. This is more complicated because the limit varies smoothly as a function of position within a given *Chandra* pointing. Deeper sensitivity limits correspond to smaller effective areas. We therefore compute *Chandra* sensitivity curves in the full band (corresponding to the selection band), accounting for the overlap with the Palomar near-IR data which is not complete over the EGS field at all depths. For a given source with X-ray luminosity L_X^i , we use a $\Gamma = 1.9$ power-law to estimate the observed flux this source would have as a function of redshift. We then use the sensitivity curve to compute the corresponding solid angle over which such a source could be detected as a function of redshift, $d\Omega(z)$. Thus, we derive a second V_{max} estimate for AGN hosts based on the X-ray limits:

$$V_{max, X-ray}^i = \int_{z_{low}}^{z_{high}} d\Omega(z) \frac{dV}{dz} dz \quad (5)$$

where z_{low} and z_{high} are given by the boundaries of the redshift interval. The final V_{max} for the AGN hosts is taken as the smaller of the V_{max} computed based on the R and K_s -band limits and $V_{max, X-ray}$. Typically the X-ray volume provides the limiting V_{max} .

The galaxy sample and AGN spec- z host sample make use of DEEP2 spectroscopic redshifts only. For this reason, additional weights must be applied to account for the redshift targeting selection function and success rate of these samples. Here we follow the technique described by Willmer et al. (2006) and modified in Bundy et al. (2006). Specifically, we compare the number of sources with good quality redshifts ($z_{quality} \geq 3$) in a given bin of $(B - R)/(R - I)/R_{AB}/K_s$ -band parameter space to the total number of sources targeted in that same bin. We adopt the ‘‘optimal’’ model of Willmer et al. (2006), which accounts for the different ways that red and blue galaxies are likely to be excluded from the spectroscopic sample.

The situation is more complicated for AGN hosts because applying this weighting scheme to AGN hosts assumes that the photometric sources in the corresponding color/magnitude bins also host AGNs. We therefore modify the weighting scheme when it is applied to AGN hosts as follows. In each redshift interval we determine the ratio between the number of spectroscopic AGN hosts and the number of potential hosts. Potential hosts include galaxies without X-ray detections that have spectroscopic redshifts, stellar masses greater than the completeness limit, and $U - B > -0.1$. This color requirement is motivated by Figure 2 which demonstrates that most AGN hosts have such colors. For the three redshift intervals $0.4 < z < 0.7$, $0.75 < z < 1.0$, and $1.0 < z < 1.4$, we find AGN fractions of 0.08, 0.09, and 0.14. The AGN spec- z host weights are then determined by multiplying the ‘‘optimal’’ weights discussed above by these numbers and ensuring the weight does not drop below 1.0. No weighting is required for the AGN photo- z host samples; comparisons between the spec- z and photo- z AGN host samples thus provide a useful measure of the success of our weighting scheme.

5.2. The AGN Host Stellar Mass Function

We plot the AGN spec- z and photo- z supplemented host mass functions in Figure 3 in three redshift intervals. The green shading represents the uncertainty in the spec- z sample, arising primarily from number statistics. The corresponding mass functions of the AGN photo- z host sample are indicated by asterisk symbols connected by dotted lines. For reference, each panel also indicates the total spec- z AEGIS mass function (light gray shading with solid circles), the total photo- z supplemented MF (triangle symbols), and in all panels the best fitting MF at $z \approx 0.5$ from Bundy et al. (2006). The number of AGN spec- z hosts diminishes significantly in our highest redshift bin. Interpretations at these redshifts rely on the photo- z sample only. Note that the total photo- z sample covers a larger area (by $\sim 25\%$) than the spec- z sample. Thus, slight differences in the total mass functions can arise from cosmic variance, especially in the lowest redshift interval.

At all redshifts, Figure 3 shows that the AGN host MF is roughly flat across the stellar mass range sampled. Comparing the AGN photo- z MFs, there is evidence that

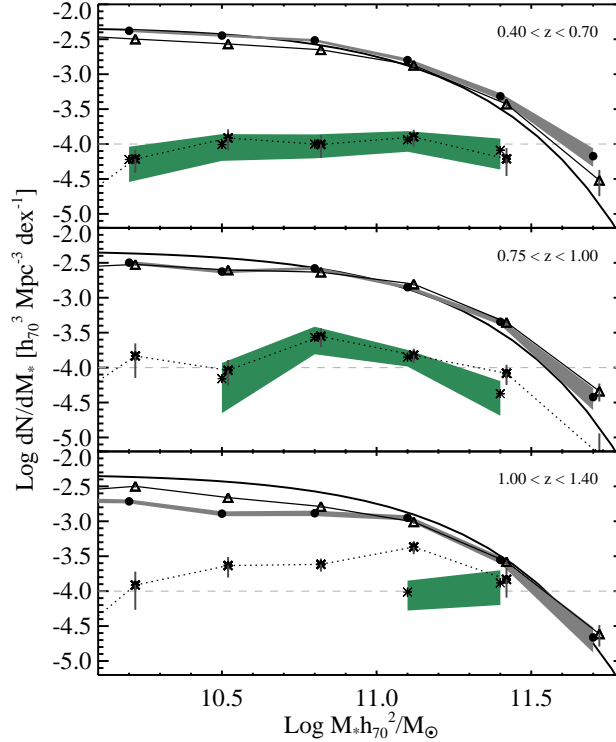


FIG. 3.— The stellar mass function of AGN host galaxies in three redshift intervals as compared to the total galaxy stellar mass function. Green shading traces the MF and uncertainty of AGN hosts with spectroscopic redshifts and $L_{2-10} > 10^{42}$ ergs s^{-1} . The asterisk symbols with error bars and connected by the dotted line show the AGN host MF for the photo- z supplemented sample. Total mass functions from the AEGIS field are shown with solid circles and grey shading (spec- z sample) and triangles (photo- z supplemented sample). The solid line is taken from the best fit of Bundy et al. (2006) to the total MF at $z \approx 0.5$. A horizontal dashed line has been drawn at $\phi = 10^{-4}$ in all panels to guide the eye.

from $z \approx 1.2$ to $z \approx 0.5$ the abundance of AGN hosts decreases roughly by a factor of 2 at all stellar masses probed. Because the corresponding number density of all galaxies is lower at $z \gtrsim 1$, the fraction of systems hosting AGNs increases at these epochs. This is shown explicitly in Figure 4 which plots the AGN fraction as a function of stellar mass. On one hand, the relatively flat MFs in Figure 3 suggest that AGN evolution—for example the declining hard X-ray luminosity density (e.g., Barger et al. 2005; Hasinger et al. 2005)—is independent of host M_* . However, the *fraction* of AGN hosts shown in Figure 4 presents a different interpretation. As galaxies continue assembling and their abundance grows with time, X-ray AGNs may be increasingly turning off—especially at the highest masses. This would lead to stronger evolution in the AGN fraction (Figure 4) accompanied by milder evolution in the absolute numbers of AGN hosts (Figure 3).

Figure 4 also shows the result of splitting the sample using two different X-ray luminosity thresholds. The dark green shading and asterisk symbols denote the AGN host sample with $L_{2-10} > 10^{42}$ ergs s^{-1} as in Figure 3. The light green shading and diamonds in Figure 4 provide a comparison to the host MF corresponding to higher X-ray luminosities of $L_{2-10} > 10^{43}$ ergs s^{-1} . Note that because of the steep decline in the X-ray luminosity function (e.g., Barger et al. 2005), the AEGIS survey area is too small to effectively sample sources with $L_{2-10} \gtrsim 10^{44}$ ergs s^{-1} .

While it appears that the more X-ray luminous AGNs are generally less abundant, we find little significant difference in the shape of the host MF as a function of X-ray luminosity. Those with $L_{2-10} > 10^{43}$ ergs s^{-1} account for roughly one-third of the full AGN sample with $L_{2-10} > 10^{42}$ ergs s^{-1} , but are associated with host galaxies with a similar mass distribution.

Studies of the AGN X-ray luminosity function (LF) show that the more luminous sources are more abundant in the past relative to the less luminous ones, a phenomenon often termed “AGN downsizing” (e.g., Hasinger et al. 2005; Barger et al. 2005). Because this trend is most apparent for systems brighter than the knee in the X-ray LF—that is AGNs with $L_{2-10} \gtrsim 10^{44}$ ergs s^{-1} —we would not expect the effect to be strong in this survey, which is too small to accurately sample such luminous AGNs. There is some suggestion, however, for this effect in the highest mass bin of the $0.7 < z < 1.0$ redshift interval in Figure 4, where it appears the most massive hosts become dominated by the brightest X-ray AGNs.

6. LINKING AGNS AND QUENCHING

We now move to the primary goal of this paper. Our aim is to evaluate the role of AGNs in the evolving star formation properties of the full galaxy population. To accomplish this, we will compare the rate at which AGNs are triggered in galaxies of a given mass with the rate at which star formation is quenched at these masses. We will use the AGN host mass function presented in the

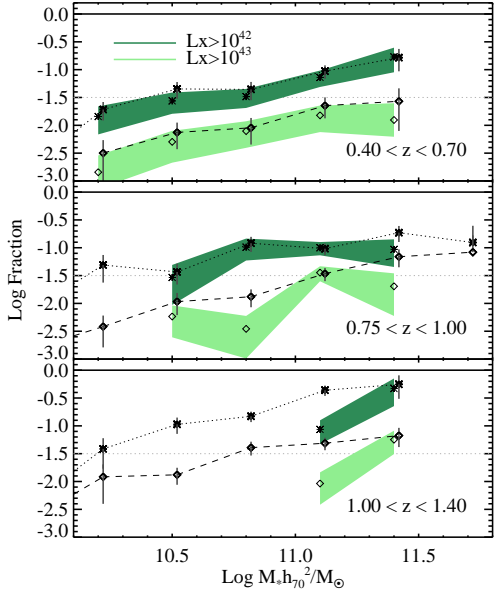


FIG. 4.— Fractional contribution of AGN hosts to the total MF in log units, shown in three redshift intervals. As in Figure 3, dark green shading denotes the AGN spec- z host sample with $L_{2-10} > 10^{42}$ ergs s^{-1} , while asterisk symbols connected by dotted lines denote the AGN photo- z host sample with the same L_{2-10} threshold. Light green shading corresponds to AGN spec- z hosts with the brighter X-ray cut of $L_{2-10} > 10^{43}$ ergs s^{-1} , while diamond symbols connected by dashed lines show the corresponding AGN photo- z MFs. A dotted horizontal line at $\log f = -1.5$ has been drawn in each panel to guide the eye.

previous section (coupled with the AGN lifetime) to infer the AGN trigger rate. First, however, we must characterize the mass-dependent quenching rate in the total population. We use the full Palomar/DEEP2 sample to provide this measurement below.

6.1. The Star Formation Quenching Rate

We will define the quenching rate, \dot{Q} , as the fraction of all galaxies in a stellar mass bin that shift to the red sequence per Gyr. This quantity can be derived using the methods of §5 to plot the increasing fraction of red galaxies (relative to the abundance of all galaxies) as a function of time for various bins of stellar mass (Figure 5). We will use the slope of the increasing red fraction to estimate \dot{Q} . We have chosen to study the red galaxy fraction—as opposed to absolute number densities—because this helps mitigate uncertainties caused by cosmic variance, which to first order affect the total number density measured in a given redshift interval (see Bundy et al. 2006).

The use of fractional abundances also provides a better handle on the rate at which galaxies become red, that is \dot{Q} . In the absence of processes that shift galaxies into different mass bins, quenching only alters the fraction of red galaxies in a given M_* bin. The transfer of galaxies across mass bins is constrained to be small by the lack of significant evolution in the shape of the total MF from $z \sim 1$. However, it is possible that both star formation and merging may move galaxies between mass bins. As for merging, we make the assumption that the effect on the red fraction is small if merging is independent of galaxy type and the merging rate does not vary across

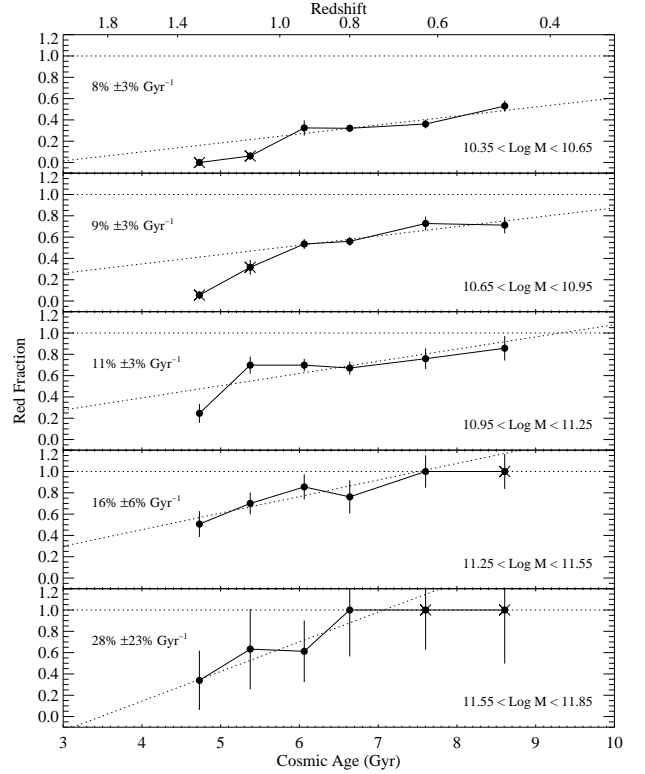


FIG. 5.— Evolving fraction of red galaxies as a function of time in various mass bins. The growing fractions have been fit by the dotted lines, excluding data points where the fraction is either 1.0 or the data are incomplete. Excluded data points are indicated by the cross symbols.

the 0.3 dex mass bins used here. As for star formation, because lower mass galaxies exhibit higher SF rates, their evolution would tend to drive the red fraction down as low mass blue galaxies enter a given mass bin. However, as the number of galaxies forming stars at a rate sufficient to double their mass over a few Gyr is small for $M_* \gtrsim 10^{10} M_{\odot}$ (e.g., Feulner et al. 2005), such an effect would have a small impact on the red fraction. Still, we emphasize that the evolving red fraction in specific mass bins is only an estimate of the true quenching rate.

The buildup in the fraction of red systems is clear in Figure 5 and allows us to crudely fit lines to the fractional growth rate. In this fit, we exclude points at early times and low masses that fall below our expected completeness limit as well as those points for which the red fraction is equal to 1.0. We take the slope of these lines as our estimate of \dot{Q} . In the mass bins centered at $\log M_*/M_{\odot} = 10.5, 10.8, 11.1, 11.4, 11.7$ we find fractional quenching rates, $\dot{Q}(M_*)$, of $8\% \pm 3\%$, $9\% \pm 3\%$, $11\% \pm 3\%$, $16\% \pm 6\%$, and $28\% \pm 23\%$ per Gyr. While Figure 5 shows that our linear approximation adequately fits the data, we cannot further constrain the quenching rates as a function of time (or redshift). Our results are obviously only valid until the red fraction reaches 1.0 and all systems are quenched and, extrapolating the fits, we find that “total quenching” in these mass intervals occurs when $z = -0.4, 0.0, 0.4, 0.6, 0.7$, or in the assumed cosmology, when the cosmic age equals $\tau_{age} = 14.7, 11.4, 9.3, 7.5, 7.3$ Gyr. Figure 5 not only reinforces the notion

that more massive galaxies become quenched first, but demonstrates the new result that they may also become quenched *faster* than their lower mass counterparts.

6.2. Comparing AGN Triggering and Star Formation Quenching

With the star formation quenching rate measured above, we now utilize the AGN host mass function to derive the AGN “trigger rate”, $\dot{\chi}(M_*)$, defined as the fraction of all galaxies per Gyr in which X-ray detected AGNs turn on as a function of stellar mass. The rate of AGN triggering multiplied by the timescale over which AGNs are visible at X-ray wavelengths is equal to the observed AGN fraction (shown in Figure 4). If we account for the AGN detection efficiency, ϵ , of our X-ray observations, we can write this relation as $f_{\text{AGN}}(M_*) = \epsilon \dot{\chi}(M_*) \tau_{\text{AGN}}$, where τ_{AGN} is the X-ray AGN timescale.

This timescale is the largest uncertainty in the calculation and must be derived from theoretical arguments. We will consider three estimates taken from the literature for the average value of τ_{AGN} . From the detailed simulations studied in Hopkins et al. (2005b) we find $\tau_{\text{AGN}} \approx 0.6$ Gyr. From the statistical and population arguments for low efficiency AGNs in Marconi et al. (2004) we use $\tau_{\text{AGN}} \approx 0.9$ Gyr, and from the model discussed in Granato et al. (2004) we use $\tau_{\text{AGN}} \approx 1.8$ Gyr. We will return to the timescale problem and discuss these estimates further below.

Assuming $\epsilon = 1$ we solve for the corresponding trigger rates, $\dot{\chi}(M_*)$, by dividing the AGN host fraction ($L_{2-10} > 10^{42}$, Figure 4) by the timescales above. We plot the results for the two redshift bins where our sample is most complete in Figure 6. The corresponding star formation quenching rates from our analysis of red galaxies is denoted by the red shaded region. The effect of a lower detection efficiency of $\epsilon \approx 0.7$ (as might arise from missed Compton-thick sources) increases the trigger rates as roughly shown by the arrow.

Despite the uncertainties and assumptions, Figure 6 demonstrates surprising agreement in both the normalization and mass dependence of the rates of quenching and AGN triggering, given the three estimates for τ_{AGN} . We interpret this as strong but circumstantial evidence that the quenching of star formation and AGN activity are physically related. We will turn to the question of whether AGNs actually *cause* quenching in §6.4.

6.3. The X-ray AGN Timescale

Because the calculation of the AGN trigger rates shown in Figure 6 relies heavily on the assumed value of τ_{AGN} , in this section we further explore the X-ray AGN timescale and the reliability of the estimates we have used. As a point of reference, we begin by deriving the value of τ_{AGN} that would be necessary to *force* the observed quenching and triggering rates to be equal. We set $\dot{Q}(M_*) = \dot{\chi}(M_*)$ and solve for τ_{AGN} at each stellar mass bin where estimates of the two rates are available (essentially we divide the full AGN host fraction in Figure 4 by the quenching rates derived in Figure 5). In principle τ_{AGN} may be related to the host stellar mass, but we will ignore this and average over the values of τ_{AGN} derived for each mass bin to roughly estimate the range or “probability distribution” of timescales needed to perfectly match the

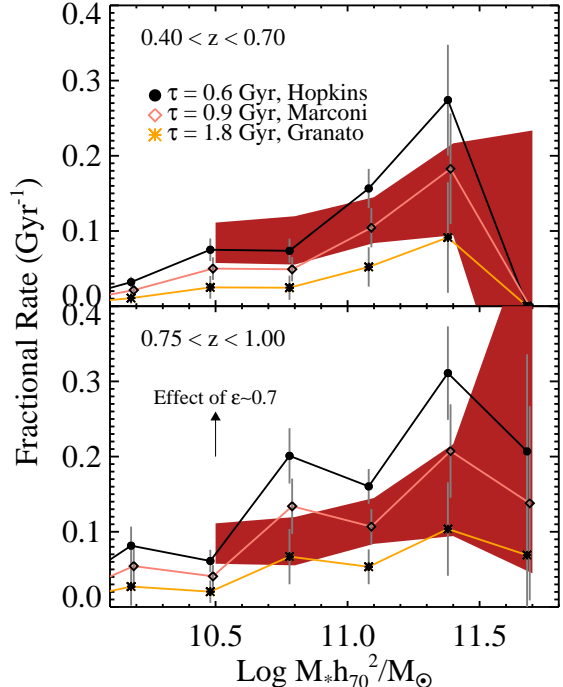


FIG. 6.— Comparison in two redshift bins between the fractional AGN “trigger rates”—calculated using three estimates of the X-ray AGN timescale—and the star formation quenching rate denoted by the red shaded region. The width of the shading illustrates the 1σ uncertainty. Trigger rates are derived based on the AGN photo- z sample (similar results are obtained for the spec- z sample), assuming all AGNs are detected and X-ray AGN timescales of 0.6, 0.9, and 1.8 Gyr based on estimates from the work of Hopkins et al. (2005b), Marconi et al. (2004), and Granato et al. (2004). The systematic effect of a 70% detection efficiency ($\epsilon \approx 0.7$) is shown by the arrow

quenching and AGN trigger rates observed in our two redshift intervals. These are plotted as the solid and dashed red lines in Figure 7 and illustrate where theoretical estimates of τ_{AGN} would fall if it were true that $\dot{Q}(M_*) = \dot{\chi}(M_*)$.

We can now compare the estimates of τ_{AGN} we have used and discuss their uncertainties. The most appropriate predictions come from detailed simulations analyzed by Hopkins and collaborators. Hopkins et al. (2005b) conduct five hydrodynamical simulations of gas rich mergers of disk galaxies that host super massive black holes (SMBHs). During the simulations, gas becomes funneled to the center of the system, fueling the growth of the newly merged SMBH. The authors use a prescription in which some fraction ($\epsilon_r = 0.1$) of this accreted material is radiated in a quasar phase. They assume 5% of this energy couples to the surrounding gas, helping to regulate the flow. The X-ray luminosity (and column density) as a function of time is calculated by assuming a quasar continuum SED and ray-tracing many lines of sight through the gas and dust in the simulated galaxy. Their Figure 2 presents a relation between the observed AGN lifetime (τ_{AGN}) and its X-ray luminosity. By applying this relation to the X-ray luminosities observed in our sample we derive a rough distribution of predicted AGN timescales which we plot as the dotted line in Figure 7. Note that the predicted τ_{AGN} from

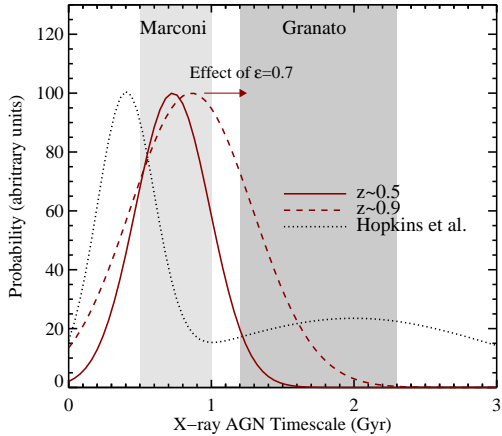


FIG. 7.— Range of X-ray detectable AGN timescales. As a reference point, the result of *assuming* the AGN trigger rate equals the quenching rate yields timescales in the range indicated by the red solid ($z \sim 0.5$) and dashed ($z \sim 0.9$) distributions. The effect of a 70% AGN detection efficiency ($\epsilon = 0.7$) on these distributions is shown by the red arrow. Independent predictions of τ_{AGN} based on the models of Hopkins et al. (2005b) have a range indicated by the dotted line. Predictions from Granato et al. (2004) and Marconi et al. (2004) are denoted by the grey shaded regions.

the Hopkins et al. (2005b) models increases rapidly for AGNs with $L_X \lesssim 5 \times 10^{42}$ ergs s^{-1} , accounting for the tail towards longer lifetimes shown in the figure and yielding the estimate of $\tau_{\text{AGN}} \approx 0.6$ Gyr used in Figure 6.

The work of Granato et al. (2004) provides another independent comparison, also based on numerical simulations that encode the effects of star formation, cooling, supernovae feedback, and AGN feedback set in the context of dark matter halos. The systems analyzed in Granato et al. (2004) are non-interacting spheroidal galaxies as opposed to merging disks, however, and while the simulations lack detailed modelling of the AGN X-ray emission, some rough constraints can be obtained for the predicted values of τ_{AGN} . Their Figure 3 shows the black hole accretion rate as a function of cosmic time in their simulations. Since, as we show below, our AGNs are likely accreting at significantly sub-Eddington rates, a rough estimate of τ_{AGN} from Granato et al. (2004) can be gained by measuring the time between peak black hole accretion in their simulations and the point at which the accretion drops below a factor 0.01–0.001 of the maximum rate. This yields AGN timescales between ~ 1 and ~ 2 Gyr as shown in Figure 7 by the grey shaded region. For an average value from Granato et al. (2004) we take $\tau_{\text{AGN}} \approx 1.8$ Gyr.

Finally, much work has been invested in utilizing various observations to constrain the lifetime of bright quasar activity, typically resulting in values of 10^7 – 10^8 yr (see the review by Martini 2004). However, historically the focus has rested on the brightest quasar phase during which black hole growth is thought to be most rapid. This phase does not correspond to the lower accretion rates of the AGNs detected in our sample. Marconi et al. (2004), however, provide a suitable estimate based on matching the local black hole density to the AGN luminosity function. For low efficiency sources, the predicted range is $\tau_{\text{AGN}} \approx 0.5$ – 1 Gyr, weighted more towards 1 Gyr for the lowest luminosity AGNs and providing a

rough average value of $\tau_{\text{AGN}} = 0.9$ Gyr.

It is clear from Figure 7 that large uncertainties exist. Still, from the detailed analysis in Hopkins et al. (2005b) to the more approximate estimates from Marconi et al. (2004) and Granato et al. (2004), this plot demonstrates that the predicted range and uncertainty in the timescale for X-ray AGN activity using a variety of methods is at least compatible with a scenario in which AGN triggering is linked to quenching. This helps to validate the agreement seen in Figure 6. Clearly further progress in confirming this link would strongly benefit from additional detailed predictions of the X-ray properties and lifetimes of AGNs.

6.4. Is AGN Feedback Responsible For Quenching?

We have argued that the similarity in the rate of AGN triggering compared to the rate of star formation quenching suggests that the two phenomena are linked. But what is the nature of this link? Specifically, we would like to know if AGNs, perhaps through feedback mechanisms, are directly responsible for the quenching of star formation. In this section we will begin to probe this question by investigating the individual properties of our X-ray selected AGNs and how they correlate with their host galaxies.

Our strategy will be to study the SMBH accretion rates—as parametrized by the Eddington ratio—in our sample. We acknowledge that these estimates are somewhat crude and subject to systematics, but argue that they nonetheless provide important insight on how AGNs are related to the properties of their host galaxies. The Eddington ratio compares the bolometric luminosity, L_{bol} , of the AGN to the Eddington Luminosity which is simply related to the SMBH mass, $L_{\text{Edd}} = 1.25 \times 10^{38} (M_{\text{BH}}/M_{\odot})$ ergs s^{-1} . To determine M_{BH} we use the relation between K -band bulge luminosity and black hole mass calculated by Graham (2007) and based on previous work (Marconi & Hunt 2003; McLure & Dunlop 2004). Note that Woo et al. (2006) find evidence that the $z \sim 0.3$ relation is offset relative to that at $z = 0$ by a +0.6 dex increase in M_{BH} , although we do not apply this correction here. As most X-ray selected AGN hosts at the redshifts of our sample have early-type morphologies (Grogin et al. 2005; Pierce et al. 2007), we assume that the bulge-to-total ratio is 1.0, but in what follows we will demonstrate the effect of lower ratios on our results. Finally, we calculate L_{bol} by assuming a hard X-ray bolometric correction of 35 (Elvis et al. 1994). Barger et al. (2005) argue that for obscured (narrow line) AGNs, the correction should be 85 although Pozzi et al. (2007), using a sample of type-2 AGNs, find a wide range of bolometric corrections with an average of ~ 25 . Clearly the bolometric corrections are uncertain within a factor of ~ 2 –3.

Using the methods above and with the stated caveats in mind we plot the estimated Eddington ratio as a function of stellar mass in Figure 8. The X-ray luminosity range of the data is indicated, showing that more luminous AGNs tend to have more efficient accretion. The isolated error bar indicates the typical uncertainties from observational scatter, while the arrows show the effects of systematic errors in estimating the bulge luminosity and bolometric correction. The “Bulge” systematic shows what would happen if the bulge-to-total ratios were low-

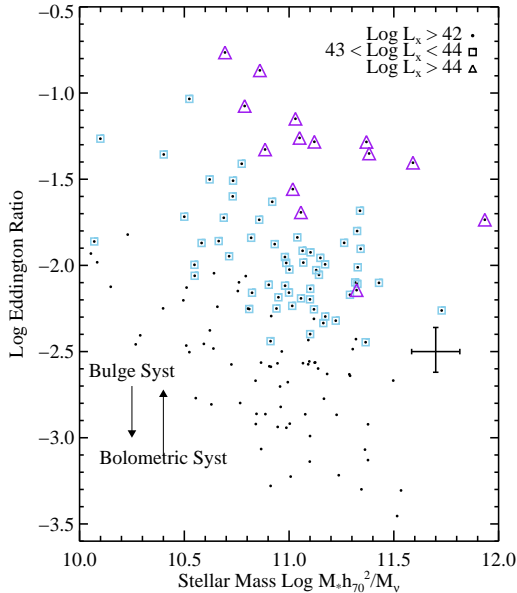


FIG. 8.— Eddington ratios in the AEGIS spec- z sample plotted against the host galaxy stellar mass. Different symbols indicate different ranges of AGN X-ray luminosity as indicated. The isolated error bar illustrates the typical uncertainty arising from observational scatter. The labelled arrows suggest the magnitude and sense of systematic uncertainties. The “Bulge” systematic shows what would happen if the bulge-to-total ratios were lowered by a factor of 2, or equivalently if the applied value of $M_{\text{BH}}/M_{\text{bulge}}$ was increased by the same amount. The “Bolometric” systematic shows the effect of increasing the bolometric correction from 35 to 85. Note that the axes are not fully independent because the Eddington ratio is proportional to M_{*}^{-1} , leading to the slight downward trend observed.

ered by a factor of 2, or equivalently if the applied value of $M_{\text{BH}}/M_{\text{bulge}}$ was increased by the same amount. The “Bolometric” systematic shows the effect of increasing the bolometric correction from 35 to 85. It is important to note that our calculation of the Eddington ratio ensures that it is proportional to M_{*}^{-1} so that downward mass-dependent trends in Figure 8 are expected given our methodology.

What is perhaps most revealing about the figure, however, is the large range (more than 2 orders of magnitude) in Eddington ratios that is apparent for host galaxies of all masses. Figure 9 shows a similar diagram where it is now possible to compare the Eddington ratios versus host galaxy restframe $(U - B)$ color. The red and blue distributions of all galaxies are indicated by the background shading. Note the existence of very blue hosts (beyond the range of normal colors) dominated by bright X-ray systems. As observed in Nandra et al. (2007), it is likely that the AGN contaminates the host color of these galaxies.

Considering the hosts in the blue cloud and red sequence, there appears to be little difference in the large spread of accretion rates. This is especially the case when one ignores the X-ray brightest systems (marked as triangles), whose true host colors may be redder than observed. We note that among all galaxies at $z \approx 0$ the fraction of dusty but still star-forming systems on the red sequence is $\sim 7\%$ and is not likely to be significantly higher at $z \sim 1$ (Yan et al. 2006). It is therefore likely that most red AGN hosts in Figure 9 are truly quenched

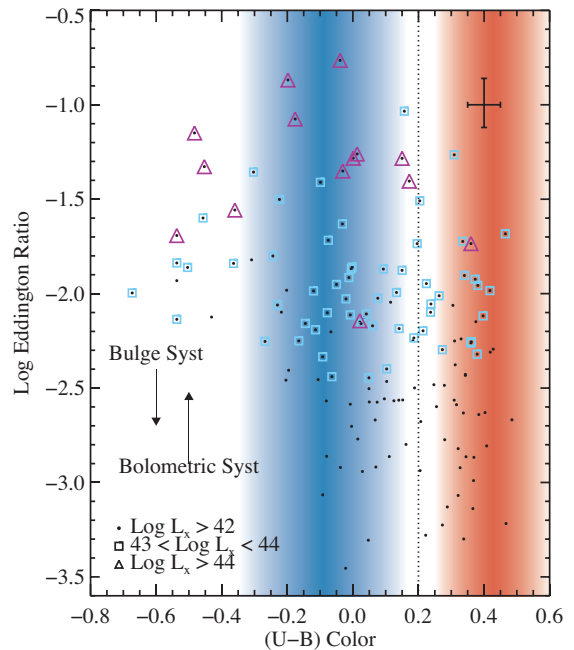


FIG. 9.— Eddington ratios as in Figure 8 for host galaxies of varying restframe $(U - B)$ color. A typical value for the division between red and blue galaxies is shown with the vertical dotted line and the color distributions of all galaxies is indicated by the background blue and red shading.

systems.

While the uncertainties in Figures 8 and 9 are large, the intrinsic scatter appears to be more substantial and suggests little or no additional trends with stellar mass or color beyond those expected from the methodology. These observations may therefore have important implications for the question of whether AGN feedback is responsible for quenching.

Some feedback models imagine that the AGN has an explosive episode that drives gas out of the galaxy halo. In the model of Hopkins and collaborators discussed above, for example, AGN activity is triggered by major mergers. The buried AGN is virtually undetectable until a violent quasar phase in which tremendous energy is expelled, sufficient to heat or disperse most of the remaining gas in the galaxy, thus quenching further star formation. As described in Hopkins et al. (2007b), in this model one would expect that AGN activity evolves with time as AGN feedback during the quasar phase impacts the surrounding material, heating and driving it from the newly merged system. The X-ray observations studied here would then correspond to the post-quasar phase tracing AGNs as they decay to low luminosities; beforehand the obscuration is predicted to be $\gtrsim 10^{24} \text{ cm}^{-2}$, enough to absorb hard X-rays. The short-lived quasar phase that immediately follows would be too bright to enable studies of host properties (see Hopkins et al. 2007b).

Figures 8 and 9 suggest some potential problems with simple interpretations of explosive models of this sort. One might expect the most massive and reddest hosts to have been quenched earliest and therefore to harbor AGNs in the latest stages of decay. Little fuel should remain in such systems long after the quasar phase, and the luminosities and Eddington ratios should be low. This picture appears consistent with observations

of local AGN hosts identified through optical emission line diagnostics. Stronger emission line AGNs are found in younger stellar populations with higher specific star formation rates, while weaker AGNs favor hosts that have apparently been quenched (Kauffmann et al. 2003; Salim et al. 2007). Figures 8 and 9 show that X-ray selected AGNs may present a different picture. Here, the reddest and most massive hosts harbor AGNs that cover nearly the full range of X-ray luminosity and accretion rates. Indeed, Figure 3 demonstrates that AGNs are hosted by galaxies with masses covering the full range probed.

One perspective on this question is suggested by the work of Ciotti & Ostriker (2007) who demonstrate that X-ray luminous AGN activity as well as starbursts can be effectively fueled by stellar mass loss from evolved stars in old stellar populations. While it is not clear what timescales would be involved, in the absence of other fueling mechanisms, this process requires an old stellar population to function, generating an obvious link between quenching and the appearance of AGNs. The work of Ciotti & Ostriker (2007) serves to demonstrate that AGNs may be fueled by a variety of mechanisms. Even if a high-accretion quasar phase was initially responsible for disrupting the internal gas supply, the AGN may later be “refueled” by such mechanisms, including the inflow of gas lost from evolved stars.

Finally, in addition to refueling, an alternative explanation for the range of AGN properties observed in the most massive and reddest hosts could come from the notion that AGN feedback is *not* responsible for quenching star formation, but is triggered by the same process that is. A nuclear starburst fueled by the same inflowing gas that ignites the AGN is a promising example, capable of providing the feedback energy necessary (in the form of stellar winds) to heat and expel the surrounding gas supply and help regulate correlations between bulge and SMBH properties (see Ferrarese & Ford 2005). Previous work has revealed evidence for a connection between starbursts and AGN activity (e.g., Yan et al. 2006; Goto 2006; Yang et al. 2006; Wild et al. 2007; Georgakakis et al. 2007a) which has also been explored in models (e.g., Somerville et al. 2001; Hopkins et al. 2007a).

A mixed AGN/starburst scenario is supported by the observations presented here. AGN activity could be initially triggered during or towards the end of starburst quenching, leading to a greater diversity in the phases of X-ray detected AGN activity among galaxy hosts. As suggested by Croton et al. (2006), low luminosity AGNs—undetected in the current sample—may be ubiquitous in quenched systems (e.g., Salim et al. 2007), providing the necessary feedback that prevents further star formation. As part of this feedback cycle, these systems could periodically enter active phases that could be detected through X-ray emission.

7. SUMMARY

We have used the combination of the DEEP2 Galaxy Redshift Survey, Palomar near-IR imaging, and *Chandra* X-ray observations to study the properties of galaxies that host X-ray selected AGNs. We summarize our findings below.

- The AGN host stellar mass function over the redshift range $0.4 < z < 1.4$ is roughly flat as a function of M_* . The abundance of AGNs appears higher at $z \sim 1$ by a factor of ~ 2 . Coupled with the decrease in number density of all galaxies at high redshift, the AGN fraction increases at early times, especially among the most massive galaxies.
- The MF of host galaxies for an X-ray luminous subset of our sample with AGN luminosities of $L_{2-10} > 10^{43}$ ergs s⁻¹ indicates a lower abundance but a very similar mass dependence as the full sample with $L_{2-10} > 10^{42}$ ergs s⁻¹. We see some evidence, however, that brighter AGNs, whose abundance increases with redshift, are hosted by more massive galaxies.
- Using the full DEEP2/Palomar sample we estimate the star formation quenching rate, defined as the number of galaxies that move to the red sequence per Gyr. Our estimates suggest that massive galaxies not only populated the red sequence at earlier epochs but did so at a faster rate than less massive galaxies.
- We show that the quenching rate agrees with the rate at which AGN activity is triggered in galaxies if the lifetime over which AGNs would be detected through X-ray emission is 0.5–1 Gyr, similar to estimates from detailed predictions based on numerical simulations and black hole demographics. The agreement between the mass-dependent quenching and AGN triggering rates is evidence of a physical link between these two phenomena.
- We test the causality of this link by comparing black hole accretion rates to the stellar mass and color of associated host galaxies. The most massive and red hosts—which presumably have quenched at the earliest times—harbor X-ray selected AGNs as active as those found in blue hosts. This suggests a more complicated relationship between AGNs and star formation. It is possible that X-ray selected AGNs are associated with but do not directly *cause* star formation quenching and, furthermore, may be subject to refueling after quenching occurs.

We would like to thank Ray Carlberg for useful discussions on this project. KB would like to acknowledge support from Olivier Le Fèvre and the Observatoire Astronomique de Marseille Provence where he was a visiting researcher. The Palomar Survey was supported by NSF grant AST-0307859 and NASA STScI grant HST-AR-09920.01-A. Support from National Science Foundation grants 00-71198 to UCSC and AST 00-71048 to UCB is also gratefully acknowledged. Financial support has also been provided through PPARC and the Marie Curie Fellowship grant MEIF-CT-2005-025108 (AG), the Leverhulme trust (KN), the Hubble Fellowship grants HF-01165.01-A (JAN) and HF-01182.01-A (ALC) and the STFC (EL). We wish to recognize and acknowledge the highly significant cultural role and reverence that the summit of Mauna Kea has always had within the indigenous Hawaiian community. It is a privilege to be

given the opportunity to conduct observations from this mountain.

REFERENCES

- Barger, A. J., Cowie, L. L., Mushotzky, R. F., Yang, Y., Wang, W.-H., Steffen, A. T., & Capak, P. 2005, *AJ*, 129, 578
- Bauer, F. E., Alexander, D. M., Brandt, W. N., Schneider, D. P., Treister, E., Hornschemeier, A. E., & Garmire, G. P. 2004, *AJ*, 128, 2048
- Bell, E. F., Wolf, C., Meisenheimer, K., Rix, H.-W., Borch, A., Dye, S., Kleinheinrich, M., Wisotzki, L., & McIntosh, D. H. 2004, *ApJ*, 608, 752
- Benítez, N. 2000, *ApJ*, 536, 571
- Bertin, E. & Arnouts, S. 1996, *A&AS*, 117, 393
- Borch, A. et al. 2006, *A&A*, 453, 869
- Bower, R. G. et al. 2006, *MNRAS*, 370, 645
- Bruzual, G. & Charlot, S. 2003, *MNRAS*, 344, 1000
- Bundy, K., Ellis, R. S., & Conselice, C. J. 2005, *ApJ*, 625, 621
- Bundy, K. et al. 2006, *ApJ*, 651, 120
- Canalizo, G. & Stockton, A. 2001, *ApJ*, 555, 719
- Cattaneo, A., Dekel, A., Devriendt, J., Guiderdoni, B., & Blaizot, J. 2006, *MNRAS*, 370, 1651
- Chabrier, G. 2003, *PASP*, 115, 763
- Cimatti, A., Daddi, E., & Renzini, A. 2006, *A&A*, 453, L29
- Ciotti, L. & Ostriker, J. P. 2007, *ApJ*, 665, 1038
- Coil, A. L., Newman, J. A., Kaiser, N., Davis, M., Ma, C.-P., Kocevski, D. D., & Koo, D. C. 2004, *ApJ*, 617, 765
- Collister, A. A. & Lahav, O. 2004, *PASP*, 116, 345
- Conselice, C. J. et al. 2007, preprint (arXiv0708.1040), 708
- Cooper, M. C. et al. 2007, preprint (arXiv0706.4089), 706
- Cowie, L. L., Songaila, A., Hu, E. M., & Cohen, J. G. 1996, *AJ*, 112, 839
- Croton, D. J. et al. 2006, *MNRAS*, 365, 11
- Cuillandre, J.-C., Luppino, G., Starr, B., & Isani, S. 2001, in SF2A-2001: Semaine de l’Astrophysique Française, 605–+
- Davis, M., Gerke, B. F., Newman, J. A., & the Deep2 Team. 2005, in ASP Conf. Ser. 339: Observing Dark Energy, ed. S. C. Wolff & T. R. Lauer, 128–+
- Davis, M. et al. 2003, in Discoveries and Research Prospects from 6- to 10-Meter-Class Telescopes II. Edited by Guhathakurta, Puragra. Proceedings of the SPIE, Volume 4834, pp. 161–172 (2003), 161–172
- Davis, M. et al. 2007, *ApJ*, 660, L1
- de Lucia, G. & Blaizot, J. 2007, *MNRAS*, 375, 2
- Dunlop, J. S., McLure, R. J., Kukulka, M. J., Baum, S. A., O’Dea, C. P., & Hughes, D. H. 2003, *MNRAS*, 340, 1095
- Elvis, M. et al. 1994, *ApJS*, 95, 1
- Faber, S. M. et al. 2007, *ApJ*, 665, 265
- Ferrarese, L. & Ford, H. 2005, *Space Science Reviews*, 116, 523
- Feulner, G., Gabasch, A., Salvato, M., Drory, N., Hopp, U., & Bender, R. 2005, *ApJ*, 633, L9
- Georgakakis, A. et al. 2006, *MNRAS*, 371, 221
- . 2007a, in prep., 660, L15
- . 2007b, *ApJ*, 660, L15
- Gerke, B. F. et al. 2007, *MNRAS*, 376, 1425
- Gilli, R., Comastri, A., & Hasinger, G. 2007, *A&A*, 463, 79
- Goto, T. 2006, *MNRAS*, 369, 1765
- Graham, A. W. 2007, *MNRAS*, 543
- Granato, G. L., De Zotti, G., Silva, L., Bressan, A., & Danese, L. 2004, *ApJ*, 600, 580
- Grogin, N. A. et al. 2005, *ApJ*, 627, L97
- Guainazzi, M., Matt, G., & Perola, G. C. 2005, *A&A*, 444, 119
- Hasinger, G., Miyaji, T., & Schmidt, M. 2005, *A&A*, 441, 417
- Hopkins, P. F., Cox, T. J., Keres, D., & Hernquist, L. 2007a, preprint (arXiv0706.1246), 706
- Hopkins, P. F., Hernquist, L., Cox, T. J., & Keres, D. 2007b, preprint (arXiv0706.1243), 706
- Hopkins, P. F., Hernquist, L., Martini, P., Cox, T. J., Robertson, B., Di Matteo, T., & Springel, V. 2005a, *ApJ*, 625, L71
- Hopkins, P. F. et al. 2005b, *ApJ*, 630, 705
- Hutchings, J. B., Cherniawsky, A., Cutri, R. M., & Nelson, B. O. 2006, *AJ*, 131, 680
- Ilbert, O. et al. 2006, *A&A*, 457, 841
- Juneau, S. et al. 2005, *ApJ*, 619, L135
- Kannappan, S. J. & Gawiser, E. 2007, *ApJ*, 657, L5
- Kauffmann, G. et al. 2003, *MNRAS*, 346, 1055
- Maraston, C. et al. 2006, *ApJ*, 652, 85
- Marconi, A. & Hunt, L. K. 2003, *ApJ*, 589, L21
- Marconi, A., Risaliti, G., Gilli, R., Hunt, L. K., Maiolino, R., & Salvati, M. 2004, *MNRAS*, 351, 169
- Martin, D. C. et al. 2007, preprint (astro-ph/0703281)
- Martini, P. 2004, in Coevolution of Black Holes and Galaxies, ed. L. C. Ho, 169–+
- McLure, R. J. & Dunlop, J. S. 2004, *MNRAS*, 352, 1390
- Mushotzky, R. 2004, in *Astrophysics and Space Science Library*, Vol. 308, *Astrophysics and Space Science Library*, ed. A. J. Barger, 53–+
- Nandra, K. & Pounds, K. A. 1994, *MNRAS*, 268, 405
- Nandra, K. et al. 2005, *MNRAS*, 356, 568
- . 2007, *ApJ*, 660, L11
- Pierce, C. M. et al. 2007, *ApJ*, 660, L19
- Pozzi, F. et al. 2007, *A&A*, 468, 603
- Salim, S. et al. 2007, preprint (0704.3611), 704
- Scannapieco, E., Silk, J., & Bouwens, R. 2005, *ApJ*, 635, L13
- Schmidt, M. 1968, *ApJ*, 151, 393
- Silk, J. & Rees, M. J. 1998, *A&A*, 331, L1
- Somerville, R. S., Primack, J. R., & Faber, S. M. 2001, *MNRAS*, 320, 504
- Treister, E. & Urry, C. M. 2006, *ApJ*, 652, L79
- Treu, T., Ellis, R. S., Liao, T. X., & van Dokkum, P. G. 2005, *ApJ*, 622, L5
- van Dokkum, P. G., Franx, M., Fabricant, D., Illingworth, G. D., & Kelson, D. D. 2000, *ApJ*, 541, 95
- Wild, V., Kauffmann, G., Heckman, T., Charlot, S., Lemson, G., Brinchmann, J., Reichard, T., & Pasquali, A. 2007, preprint (arXiv0706.3113), 706
- Willmer, C. N. A. et al. 2006, *ApJ*, 647, 853
- Wilson, J. C. et al. 2003, in *Instrument Design and Performance for Optical/Infrared Ground-based Telescopes*. Edited by Iye, Masanori; Moorwood, Alan F. M. Proceedings of the SPIE, Volume 4841, pp. 451–458 (2003), 451–458
- Woo, J.-H., Treu, T., Malkan, M. A., & Blandford, R. D. 2006, *ApJ*, 645, 900
- Yan, R., Newman, J. A., Faber, S. M., Konidaris, N., Koo, D., & Davis, M. 2006, *ApJ*, 648, 281
- Yang, Y., Tremonti, C. A., Zabludoff, A. I., & Zaritsky, D. 2006, *ApJ*, 646, L33